Volume 3 | Number 31 | 21 August 2015 | Pages 6393–6538

Journal of Materials Chemistry B

Materials for biology and medicine

www.rsc.org/MaterialsB

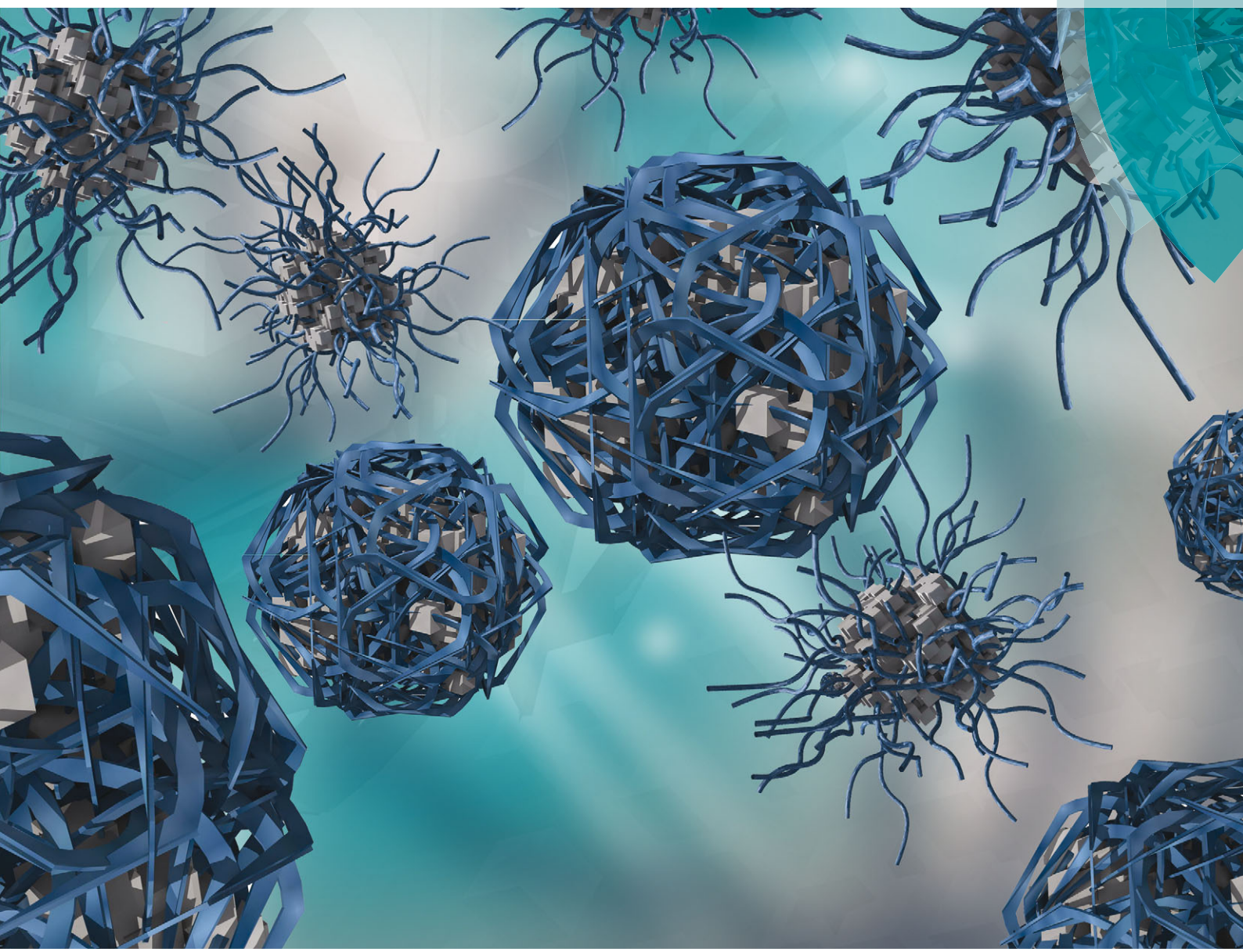

ISSN 2050-750X

ROYAL SOCIETY OF CHEMISTRY

PAPER

Keisha B. Walters *et al.*

Fetuin-A adsorption and stabilization of calcium carbonate nanoparticles in a simulated body fluid

Journal of Materials Chemistry B

PAPER

View Article Online
View Journal | View Issue

Cite this: J. Mater. Chem. B, 2015, 3, 6411

Fetuin-A adsorption and stabilization of calcium carbonate nanoparticles in a simulated body fluid†

Erick S. Vasquez,[a] Janice L. Cunningham,[b] Justin B. McMahan,[b] C. LaShan Simpson[b] and Keisha B. Walters*[a]

Received 29th March 2015,
Accepted 3rd July 2015

DOI: 10.1039/c5tb00565e

www.rsc.org/MaterialsB

Fetuin-A is a serum glycoprotein identified as a calcification inhibitor, and a key player in bone formation and human metabolic processes. A study on binding mechanisms of Fetuin-A with calcium carbonate nanoparticles in a simulated body fluid (DMEM) environment is presented. Observed interactions between Fetuin-A and the $CaCO_3$ nanoparticles reveal an initial adsorption process, followed by a stabilization stage, and then a solubilization period for the Fetuin-A/$CaCO_3$ complex. FTIR and XPS are used to monitor functional group and elemental composition changes during the initial adsorption process between Fetuin-A and the $CaCO_3$ nanoparticles. Distinctive Fetuin-A/$CaCO_3$ complex structures—also known as mineralo-protein particles—are imaged with TEM and SEM. DLS and UV-Vis methods are used to further characterize the *in situ* binding mechanisms. Results of this study can guide the design of complex organic–inorganic hybrid materials, improve current drug delivery methods, and provide insight in monitoring and controlling interactions between Fetuin-A and external calcium ions.

1. Introduction

Composites where the individual materials have micro-to-nano length scales have demonstrated many advantages over single-material synthetic materials, including properties such as biocompatibility, stability, dispersion, and surface-functionalities that can be manipulated and enhanced.[1–4] For example, biocomposites—inorganic materials combined with proteins, natural polymers, or other biomolecules—display greater biocompatibility than solely inorganic, synthetic materials.[5] Furthermore, small length scales of the composite components supports the mimicking of natural mechanisms which occur in the formation of organic biocomposites (*e.g.*, crustaceans, shell-fish, skeletal bone).[4–8] Moving beyond the realm of 'bioinspired' to the development of novel 'self-functioning' materials, which utilize inherent chemical and biological mechanisms to carry out specific functions, allows for enhanced dynamic processes such as self-assembly, reversible adsorption/desorption, and solids precipitation and resolubilization to occur.[9–11]

This work examines biomineral formation and remodeling; specifically focusing on the role of proteins on stabilizing the formation and solubilization of calcium nanoparticles. Key players in the skeletal biomineralization process have been shown to also play a significant role in the development of pathological vascular calcification.[12] For instance, proteins regulate bone growth and remodeling by actively inhibiting or promoting mineral deposition and cell mediated activities. These regulatory mechanisms may be effective at treating vascular calcification given its similarity to bone biomineralization.[13] Additionally, an understanding of the interactions between proteins and mineral nuclei is necessary for the development of protein–nanoparticle therapies that can effectively treat and potentially reverse vascular calcification. For example, protein–mineral interactions observed in biomineralization have been utilized to design novel nanoparticle-protein adsorption techniques for the development of drug delivery systems, theranostic procedures, and gene therapy for the transport of biological macro-molecules into cells and tissues.[14–16] The important role of acidic proteins in the structure and mineralization of calcified tissues has long been recognized; however, the relationship between proteins and their precise function in (de)mineralization processes remains obscure.[17]

Fetuin-A, also known as α-2-Heremans Schmid glycoprotein (AHSG), is a well-studied acidic serum glycoprotein and physiological regulator of bone metabolism. Many studies suggest

[a] Dave C. Swalm School of Chemical Engineering, Mailstop 9595, 330 Swalm Chemical Eng. Bldg., Mississippi State, MS, 39762, USA. E-mail: kwalters@che.msstate.edu
[b] Agricultural and Biological Engineering Department, Mailstop 9632, 130 Creelman St., Mississippi State, MS, 39762, USA

† Electronic supplementary information (ESI) available: ESI1: infrared spectroscopic analysis of $CaCO_3$ nanoparticles and Fetuin-A; ESI2: time-dependent study of Fetuin-A/$CaCO_3$ complexes; ESI3: UV-Vis absorbance of Fetuin-A, $CaCO_3$ particles, and Fetuin-A/$CaCO_3$ complexes. See DOI: 10.1039/c5tb00565e

that Fetuin-A acts as a chaperone protein that produces and stabilizes calcium phosphate mineral colloids, also referred to as calciprotein particles (CPPs) or fetuin mineral complexes (FMCs).[18] Once formed, Fetuin-A facilitates cellular resorption of CPPs; however, the exact mechanism(s) of CPPs clearance from cells has yet to be determined.[19,20] In order to further elucidate the exact mechanism of Fetuin-A inhibition and stabilization of mineral colloids, several groups have studied the ability of Fetuin-A to form CPPs under supersaturated concentrations of calcium and phosphate *in vivo* and *in vitro.* For example, Heiss *et al.* used scanning electron microscopy (SEM) to show that the addition of miniscule amounts of Fetuin-A/AHSG induced morphological changes in basic calcium phosphate precipitations that resulted in a brittle appearance of the precipitate formed.[18] Pasch *et al.* used three-dimensional cross correlation dynamic light scattering (DLS) to show that CPP formation is a time dependent biphasic process which results in morphological changes as well as an increased CPP diameter.[21] Lastly, the formation and stability kinetics of the CPPs, analyzed using time-resolved dynamic light scattering, showed CPP size and that the secondary ripening transition phase depends more on Fetuin-A/mineral concentration ratio than reaction temperature.[22]

Fetuin-A interaction and stabilizing ability with calcium phosphate is a well-known phenomenon; as such, the interest of this study is to observe whether Fetuin-A is a potent enough regulator of mineralization to control aggregation and growth of other types of calcium polymorphs. To date, there have been no experimental studies on Fetuin-A's ability to stabilize other sources of calcium, including calcium carbonate ($CaCO_3$) which has gained tremendous interest as a stabilizer for drug delivery applications.[23,24] Moreover, $CaCO_3$ biocompatibility and biodegradability has led to the development of different structures such as self-assembled nanovesicles,[23] protein adsorption/release experiments,[24] and the development of hollow microspheres.[25]

$CaCO_3$ crystalline forms (*i.e.* calcite, valerite, and aragonite) are usually obtained from an amorphous calcium carbonate (ACC) precursor which is a naturally occurring composite extensively studied during biomineralization in living organisms.[24] ACCs are also used as a template for core–shell particles,[26,27] but are thermodynamically unstable and tend to crystallize. However, researchers have discovered that in some instances transient biogenic ACC has the ability to remain stable for the entire life span of some organisms (*e.g.*, exoskeleton shells of crustaceans).[26] In particular, this work pursues to obtain a better understanding of Fetuin-A adsorption, stabilization, and solubilization of $CaCO_3$ crystals in the presence of a simulated body fluid in order to develop a protein/nanocomposite-based therapy for drug delivery applications, and to motivate further studies for possible competing effects with the well-known CPP_S.

This study focuses on the binding mechanisms of Fetuin-A, a model protein for the further understanding of acidic proteins, with $CaCO_3$ nanoparticles.[28] As biomineralization naturally occurs under supersaturated extracellular environments and in the presence of ions we wanted to study Fetuin-A interaction with mineral particles in a setting that would mimic a real-life biological system (*i.e.* blood) as closely as possible. To better understand the *in vivo* bioactivity of the Fetuin-A protein as it stabilizes and binds $CaCO_3$ particles we utilized Dulbecco's modified Eagle's medium (DMEM) as a simulated body fluid.[29–31] The overall objective of this investigation is to characterize the binding mechanisms and chemical interactions between Fetuin-A and calcium-based nanoparticles in a simulated body fluid. Specific findings presented include: (1) elucidation of the role of Fetuin-A as a model stabilizer of calcium-mineral polymorphs, including confirmation of protein adsorption and binding with $CaCO_3$ nanoparticles; (2) reporting, for the first time, infrared spectroscopic spectral signatures of Fetuin-A and the chemical changes when binding with $CaCO_3$ nanoparticles; (3) identification of morphological changes in these Fetuin-A/$CaCO_3$ nanoparticle complexes after formation; and (4) validation of protein monolayer adsorption onto $CaCO_3$ surfaces and solubilization over time utilizing *in situ* dynamic light scattering and spectroscopic methods to assess protein adsorption and time-dependent binding onto $CaCO_3$ nanoparticles.

2. Results and discussion

2.1 Chemical characterization of Fetuin-A, $CaCO_3$, and Fetuin-A/$CaCO_3$ nanoparticle complexes

The "as-received" $CaCO_3$ nanoparticles and pure Fetuin-A protein were characterized using attenuated total reflection FTIR (ATR-FTIR) spectroscopy to evaluate the infrared absorption bands corresponding to their chemical composition. $CaCO_3$ crystalline or amorphous state has been previously characterized using FTIR, as discussed elsewhere.[32–34] In this study, the "as-received' $CaCO_3$ nanoparticles were characterized with ATR-FTIR and three distinctive absorption peaks were observed. We have confirmed the presence of calcite, in its purest form, in the $CaCO_3$ nanoparticles used in this study due to the appearance of the absorption bands at 1426 cm^{-1}, 876 cm^{-1} and 712 cm^{-1} wavenumbers (Fig. 1A and Fig. S1, ESI†) corresponding to calcite stretching vibrations (ν_3, ν_2, and ν_4, respectively).[32–34] A complete spectrum, collected with a separate FTIR detector, is shown and discussed in ESI1.†

Similar characterization was performed on neat Fetuin-A and is, to the authors' knowledge, the first study reporting the infrared (IR) molecular absorptions of this glycoprotein (Fig. 1A; Fig. S2, ESI†). Typically, IR characterization of proteins is performed by deconvoluting the amide I and amide II regions of the IR spectrum.[35] This section focuses on the main differences between Fetuin-A and Fetuin-A/$CaCO_3$ through an analysis of the amide I and II spectral region (Fig. 1B and C). A full discussion of the characteristics bands of Fetuin-A is provided in ESI1, (Fig. S2 and Table S1, ESI†).

For neat Fetuin-A, the amide I region shows four distinctive peaks between 1600–1700 cm^{-1} (Fig. 1B). Two peaks corresponding to the C═O stretching vibrations were observed at 1700 cm^{-1} and at 1654 cm^{-1}, respectively. The peak at 1700 cm^{-1} is attributed to the presence of glutamic acid or aspargine aminoacids.[36] The peaks observed at 1654 cm^{-1} in the amide I

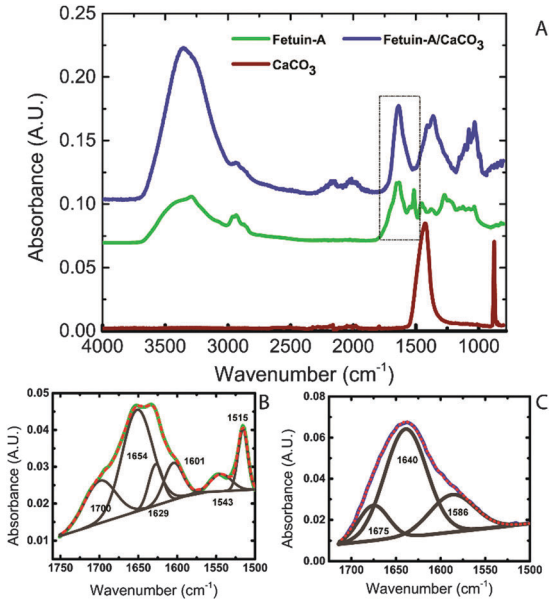

Fig. 1 ATR-FTIR spectra for (A) Fetuin-A, $CaCO_3$, and Fetuin-A/$CaCO_3$ complexes, (B) amide-I and amide-II region for neat Fetuin-A, and (C) amide-I and amide-II region showing absoprtion changes after the complexation of Fetuin-A with $CaCO_3$.

region can be assigned to an α-helix (1654 cm^{-1}) secondary protein structure and/or to the C═O stretching vibrations from arginine aminoacids.[36] Peaks for β-sheet (1629 cm^{-1}) secondary structures[35,36] intermolecular β-sheets turns (1601 cm^{-1})[35] were observed for neat Fetuin-A. Significant spectral changes were observed after the addition of Fetuin-A to the $CaCO_3$ nanoparticles.

For the Fetuin-A/$CaCO_3$ nanoparticle complex only three absorption peaks were observed, indicating binding induced changes in the chemical structure. Similar conformational changes of protein adsorption on nanoparticles using FTIR have been reported for other protein types.[37,38] For the characteristic amide I vibrations, only two peaks were identified for Fetuin-A/$CaCO_3$; located at 1640 cm^{-1} and 1675 cm^{-1} these peaks correspond to asparagine (C═O) amino acid groups.[36] This result points to a potential mechanism for Fetuin-A adsorption onto the $CaCO_3$ particles, specifically involvement of the β-sheets and α-helix turns of the protein as indicated by the loss of these amide I peaks in spectra for the Fetuin-A/$CaCO_3$ complexes. This result indicates that the acidic residues on the β-sheet structure of Fetuin-A are responsible for calcium inhibition and adsorption of the protein onto this calcium substrate, as previously discussed by Heiss *et al.*[18]

The amide II band for neat Fetuin-A shows an absorption peak at 1543 cm^{-1} (N–H) corresponding to a primary amine deformation.[36] Another peak located at 1515 cm^{-1} was also observed, and this peak can be assigned to C–O stretching in the alcohols of amino acids, such as tyr-OH or *p*-cresol (Fig. 1C).[36,39] When Fetuin-A was combined with $CaCO_3$ particles, a significant shifting of the amide II peak was observed (1586 cm^{-1}); this significant increase in wavenumber is attributed to the adsorption interactions between Fetuin-A and the $CaCO_3$ nanoparticles.[40]

Surface coverage and elemental compositions was studied using X-ray photoelectron spectroscopy (XPS) for both the "as-received" $CaCO_3$ nanoparticles and the Fetuin-A/$CaCO_3$ complexes. Fig. 2A displays representative survey scans for $CaCO_3$ nanoparticles and Fetuin-A/$CaCO_3$ complexes. Elemental surface composition for the $CaCO_3$ nanoparticles included carbon (C, 32.8 ± 3.1), calcium (Ca, 18.4 ± 3.8%), and oxygen

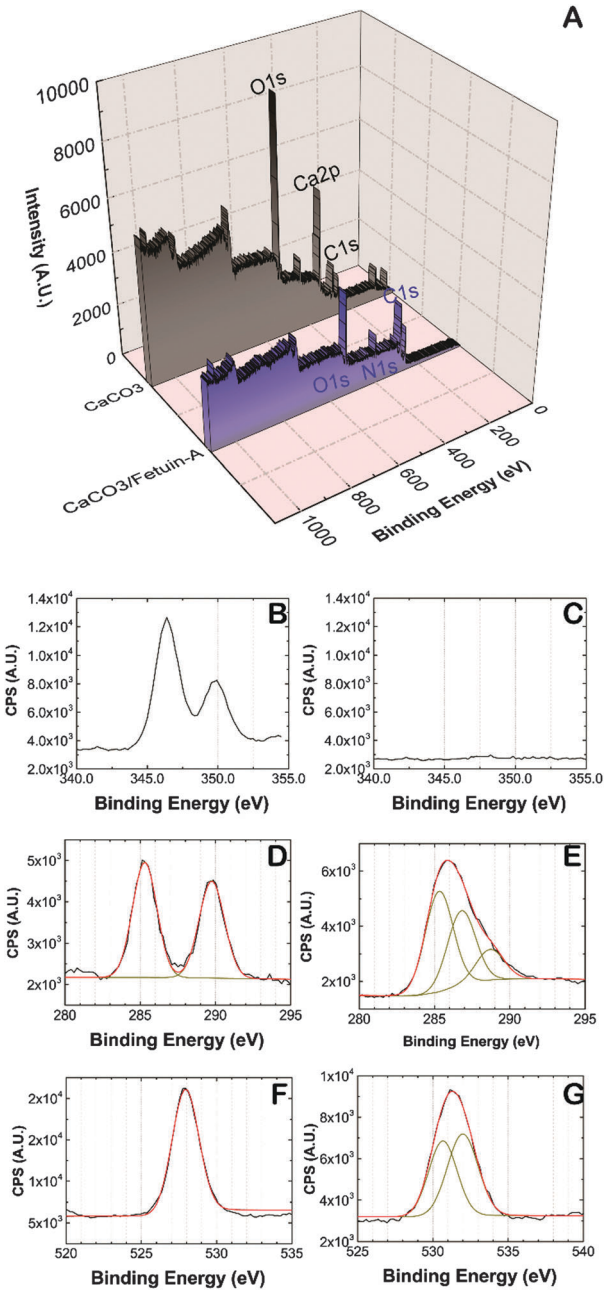

Fig. 2 (A) XPS survey scans confirming the addition of the serum glycoprotein Fetuin-A onto the surface of the $CaCO_3$ nanoparticle aggregates, as shown by the presence of nitrogen. Comparison of the high-resolution calcium, carbon, and oxygen scans for the neat $CaCO_3$ particles (B, D and F) and Fetuin-A/$CaCO_3$ complexes (C, E and G) show complete coverage of the $CaCO_3$ surface with Fetuin-A and protein-mineral binding. Nitrogen high resolution XPS scans are shown in Fig. S5 (ESI†).

(O, 48.9 ± 0.9%). Moreover, these atomic percentages are close to the theoretical atomic elemental composition of $CaCO_3$ (20% C, 20% Ca, and 60% O), confirming the presence of $CaCO_3$ as previously shown by IR analysis. The higher carbon content observed in $CaCO_3$ nanoparticles is attributed to adventitious carbon present in XPS measurements when materials are exposed to air.[41] To further investigate the atomic percentage of calcium, SEM-EDS was performed and an average value of 22.8 ± 13.2% was reported.

Elemental compositions for the Fetuin-A/$CaCO_3$ complexes were also measured and compared with XPS and SEM-EDS results. The average atomic composition reported by XPS for Fetuin-A/$CaCO_3$ was 61.4 ± 0.6% C, 31.3 ± 0.8% O, and 7.3 ± 1.5% N. The presence of nitrogen and the increase in the carbon content, despite the presence of adventitious carbon, correlates with the inclusion of glycoproteins, confirming the presence of Fetuin-A on the surface of $CaCO_3$ nanoparticles.[39] Moreover, after Fetuin-A adsorption, the presence of calcium could not be detected within the 10 nm penetration depth of XPS suggesting that $CaCO_3$ has been completely covered by a layer of Fetuin-A, a Fetuin-A/$CaCO_3$ complex structure that would result in $CaCO_3$ particle stabilization. Similarly, SEM-EDS results showed a negligible atomic percentage for Ca of 0.06 ± 0.11%, validating the surface coverage of Fetuin-A on the $CaCO_3$ nanoparticles.

High-resolution XPS identified specific functional groups and chemical bonds present as part of the chemical changes due to the formation of the Fetuin-A/$CaCO_3$ complex. Fig. 2B and C show the high resolution calcium scans for $CaCO_3$ and the Fetuin-A/$CaCO_3$ complex. For the neat $CaCO_3$ sample, two distinctive calcium peaks were observed at 246.5 and 250.0 eV, corresponding to the Ca $2p_{3/2}$ and Ca $2p_{1/2}$ photoelectron lines, respectively.[42,43] After Fetuin-A adsorption, these Ca peaks were no longer observed (Fig. 2C), demonstrating protein surface adsorption. High resolution carbon and oxygen scans were also performed (Fig. 2D–G), and adsorption-related C and O transitions observed. The C 1s peak corresponding to *C*–*C*/*C*–H bonds was observed in both samples at 285.3 eV corresponding to the carbon present in Fetuin-A, and this photoelectron line was used as a reference calibration for charge compensation.[44] An additional peak was observed at approximately 290 eV in the $CaCO_3$ sample (Fig. 2D), confirming the presence of the carbonate ($(C–O)_3$) group.[42]

Fetuin-A adsorption resulted in a number of additional C and O absorption peaks. The presence of the Fetuin-A glycoprotein on the $CaCO_3$ particles was demonstrated by the peak at 285.3 eV assigned to *C*–*C*/*C*–H bonds found in carbohydrates, proteins, lipids and hydrocarbon chains.[40,45] Additionally, the peak at 286.8 eV can be attributed to *C*–O, *C*–N and/or N–*C*–O bonds.[40,46] A second peak located at 288.7 eV corresponds to the carbon of an amide functional group (N–*C*═O), which is present in the Fetuin-A glycoprotein.[46,47] Lastly, results for the O 1s high-resolution XPS analysis on the $CaCO_3$ nanoparticles revealed a 528 eV binding energy attributable to the oxygen ($(C–O)_3$) in $CaCO_3$.[43] Due to Fetuin-A adsorption in forming the Fetuin-A/$CaCO_3$ complex, two distinctive chemical shifts were observed. The peak observed at 530.6 eV is assigned to oxygen in amino acid chains,[48] and the peak observed at 532 eV is assigned to a C═O peptide bond,[45] or possibly to residual –OH bonds after evaporation of the Dulbecco's modified Eagle's medium (DMEM).[49] Moreover, the presence of an N 1s photoelectron line confirms Fetuin-A is present on the exterior of the Fetuin-A/$CaCO_3$ complexes (additional details in Fig. S3, ESI†).[45] These XPS data corroborate the ATR-FTIR results in confirming the presence of Fetuin-A on the exterior of the Fetuin-A/$CaCO_3$ complex.

2.2 Morphological characterization of Fetuin-A, $CaCO_3$, and Fetuin-A/$CaCO_3$ complexes

The formation of organic/inorganic composites involves changes in crystal morphology and shape, with structural conformations and conditions to control changes in structure yet to be explored.[50] Fetuin-A when combined with calcium phosphate particles can produce calciprotein particles or fetuin-mineral complexes, as reported elsewhere.[18,22,51–53] In terms of morphological characterization, calciprotein particles are soluble colloidal spheres stabilized by the presence of Fetuin-A; however, formation of large precipitates (~450 nm) with radially expanded, oriented crystalline needles has been shown as a function of time.[18] Morphology of complexed Fetuin-A is important, as the structure impacts the ability to adsorb and desorb complexed minerals. Thus, while Fetuin-A has shown to act as an inhibitor of ectopic calcification, in order for Fetuin-A to selectively complex with vascular calcification the requisite complexed protein morphology(s) need to be investigated further.[22,54]

Small-angle neutron scattering data has shown that Fetuin-A does not inhibit mineral nucleation but does prevent growth and aggregation of mineral particles by covering with a layer of Fetuin-A.[55] In an effort to obtain a better understanding of the morphological structural changes of the Fetuin-A/$CaCO_3$ complexes, SEM and TEM characterization was performed. Analysis of the $CaCO_3$ particles by SEM shows a rhombohedral morphological structure (Fig. 3). Calcite crystals with a rhombohedral shape have also been reported elsewhere, confirming the crystal structure of the 'as-received' $CaCO_3$ nanoparticles.[56] Aggregation of $CaCO_3$ particles without any stabilizer present in solution was observed as the particle solution was dried on the SEM grid (Fig. 3A inset). The $CaCO_3$ particles were also investigated using TEM as shown in Fig. 4. The presence of densely packed clusters and aggregation of $CaCO_3$ was observed (Fig. 4A and B).

Rhombohedral structures can also be seen with TEM at higher magnifications (Fig. 4C) for the precipitated $CaCO_3$ particles, confirming the presence of nanosized $CaCO_3$ crystals within a larger-scale aggregated structure. These results match those in prior studies on aggregation of the mineral phase.[57] Furthermore, DLS studies are shown to confirm the aggregation of the $CaCO_3$ crystals while in DMEM solution, as discussed in Section 2.3. Our results indicate that aggregated $CaCO_3$interact with Fetuin-A proteins to form a complex. After Fetuin-A is combined with $CaCO_3$ particles, SEM (Fig. 5A and B) shows that the $CaCO_3$ nanoparticle aggregates have been stabilized by Fetuin-A. As observed in Fig. 5, spherical Fetuin-A begins to

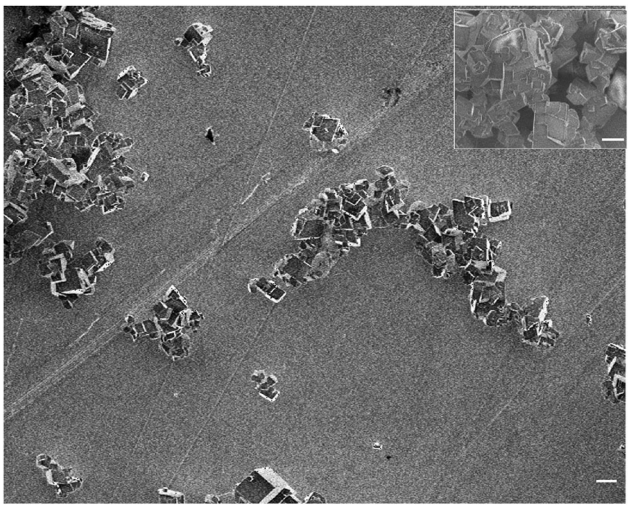

Fig. 3 SEM image of neat calcium carbonate nanoparticles demonstrating a rhombohedral crystalline structure and nanoparticle aggregation. Inset image confirms the presence of non-uniform $CaCO_3$ particles. Scale bars on the main and inset images represent 10 microns.

adsorb onto the $CaCO_3$ phase alone. These Fetuin-A/$CaCO_3$ complexes show particle sizes ranging from 400–600 nm after a two-day incubation period (Fig. 5A and B). Interestingly, the rhombohedral morphologies were no longer observed, confirming protein adsorption on the $CaCO_3$ nanoparticle aggregates.

Future studies will focus on determining the atomic arrangements and possible mechanisms by performing small-angle neutron/X-ray scattering. Previous studies have shown that calcium carbonate, in the presence of an acidic protein, binds parallel to the calcium plane, resulting in changes in the rhombohedral morphological structure and surface smoothness.[58] As observed by SEM, the $CaCO_3$ rhombohedral structures were lost when Fetuin-A/$CaCO_3$ complexes were formed (Fig. 5A and B). This matches prior literature reports and supports the deaggregation and dissociation of the $CaCO_3$ particles when Fetuin-A is surrounding the $CaCO_3$ aggregate.[59]

To examine the morphological changes within the Fetuin-A/$CaCO_3$ complexes, high-resolution TEM analysis was also conducted. Three interesting morphologies were observed which point to possible stabilization/passivation mechanisms and binding interactions between Fetuin-A and the $CaCO_3$ nanoparticle structures. First, a corona surrounding unstructured

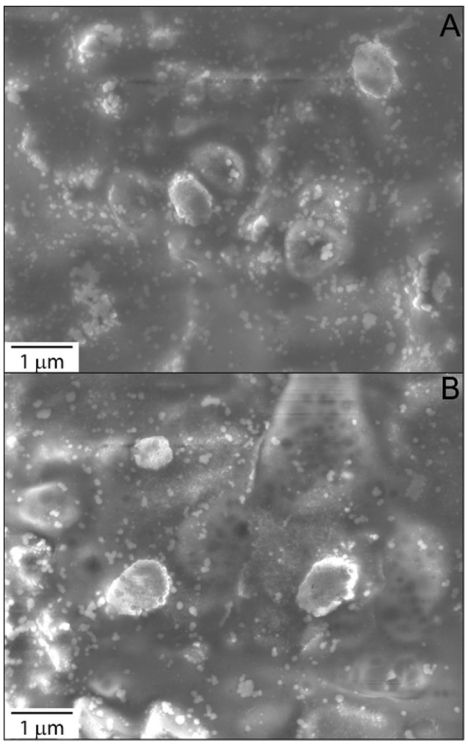

Fig. 5 SEM images of Fetuin-A/$CaCO_3$ particle-complexes demonstrate the formation of ovoid structure after Fetuin-A stabilization (A and B) in DMEM. Fetuin-A/$CaCO_3$ complexes showed different morphological forms, including large and small aggregates.

agglomerates of $CaCO_3$ particles is observed (Fig. 6A) for mature (longer incubation time) Fetuin-A/$CaCO_3$ complexes, as previously shown by neutron scattering experiments.[55]

A second morphology was observed (Fig. 6B), and is attributed to a transient state in which Fetuin-A proteins are bound to small $CaCO_3$ particles (Fig. 6B inset). Similar branches with defined orientation have been observed with hydroxyapatite crystals in the presence of special block copolymers.[60] This second morphological structure can produce more stable Fetuin-A/$CaCO_3$ complexes with ovoid structures, similar to those observed with SEM and further confirmed with DLS studies (Section 2.3). The third morphology (Fig. 6C) shows the presence of needle-like structures in the corona, a more diffuse core, and small $CaCO_3$ particles observed at the exterior

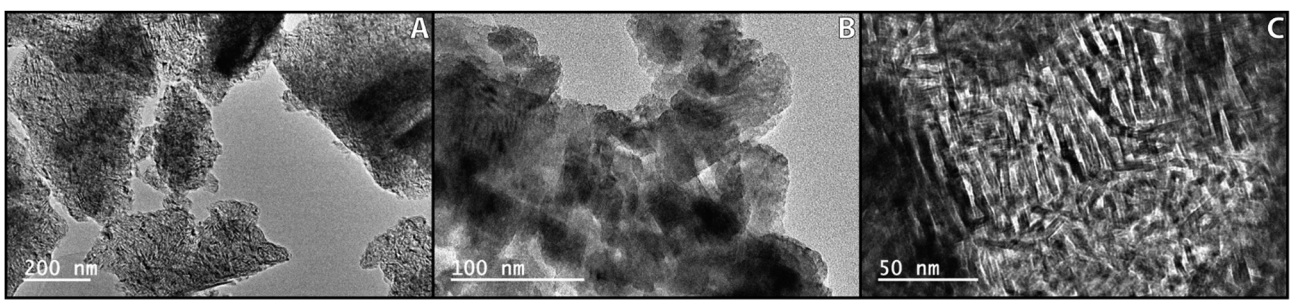

Fig. 4 TEM images of $CaCO_3$ showing aggregation (A and B). At high resolution, a rhombohedral-like structure is observed which is characteristic of calcite materials (C).

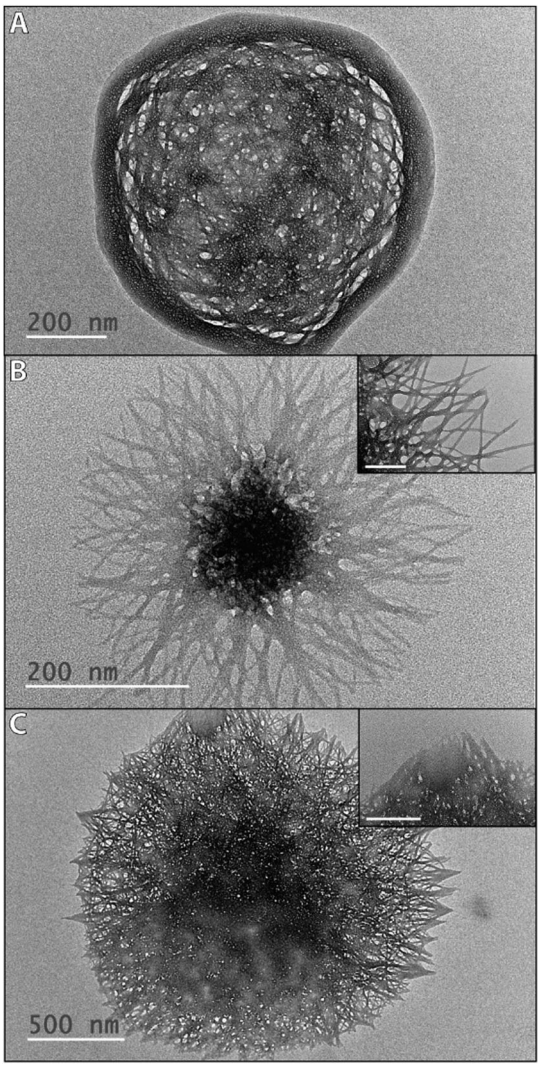

Fig. 6 Representative Fetuin-A/$CaCO_3$ complexes observed under TEM reveals the adsorption and complete surface coverage of Fetuin-A onto $CaCO_3$. $CaCO_3$ nanoparticle aggregate cores are stabilized by the surrounding protein shell (A). Possible intermediate forms (B and C) show needle-like structures (inset) formed on the periphery of large $CaCO_3$ aggregates. These intermediate forms also show calcium nano-sized spheres 'appearing to be removed from the large $CaCO_3$ core after Fetuin-A adsorption (insets). Scale bars for inset images are 200 nm.

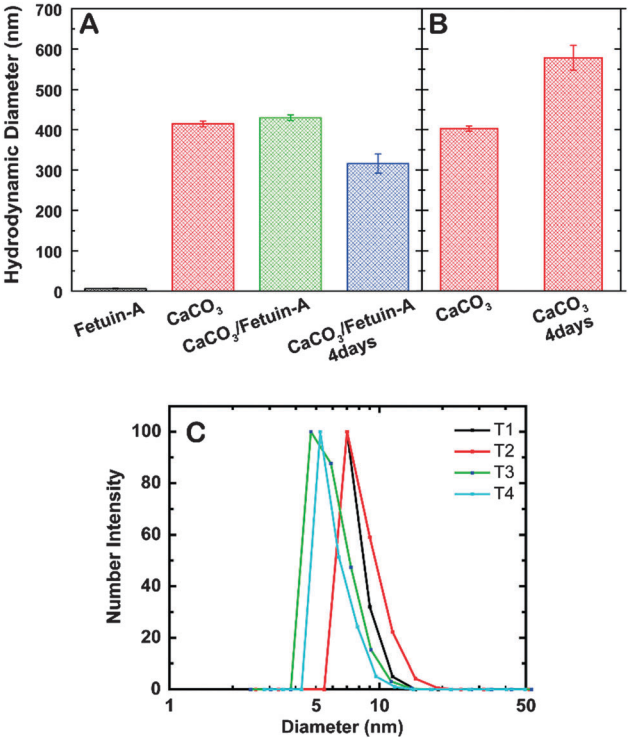

Fig. 7 (A) Average effective hydrodynamic diameter increases from the $CaCO_3$ nanoparticle aggregate to the Fetuin-A/$CaCO_3$ complex, confirming the adsorption of Fetuin-A on the surface. After a 4-day (96 h) incubation period, a significance decrease in size was observed (~27%), suggesting the removal of calcium from the complex, as indicated by TEM. (B) Neat $CaCO_3$ nanoparticles instability in DMEM and significant (43%) increase in size after a 4-day (96 h) incubation period. (C) Number intensity DLS particle size data are shown for neat Fetuin-A indicating stability in DMEM.

(Fig. 6C inset). These needle-like structures have been well-reported in the literature for the formation of calcium-protein complexes.[52] These results can aid in understanding the formation of Fetuin-A/$CaCO_3$ complexes; for instance, in this study Fetuin-A is shown to induce the formation of calcium-protein complexes with $CaCO_3$ particles without the presence of phosphate ions as reported elsewhere.[22,51,54] Thus, Fetuin-A also interacts with $CaCO_3$ in a similar fashion as hydroxyapatite crystals; thus, special considerations should be considered for the development of drug delivery vehicles consisting of $CaCO_3$ particles.

2.3 *In situ* characterization of Fetuin-A/$CaCO_3$ complexes

Dynamic light scattering (DLS) and UV-Vis spectroscopy were used to analyze the *in situ* hydrodynamic diameter and molecular absorbance of Fetuin-A and the Fetuin-A/$CaCO_3$ complexes while in an aqueous simulated body fluid (DMEM). A number-averaged particle diameter of 6 ± 0.74 nm was obtained by DLS for Fetuin-A in DMEM (Fig. 7A and C), and compares well with literature measurements of 4.2 nm for Fetuin-A corresponding to an ASHG monomer.[18]

Number-averaged mean diameters for these samples were reproducible, as shown by the plots for multiple runs (Fig. 7B). Prior studies on neat Fetuin-A showed that larger agglomerates form in aqueous solutions, and this behavior was observed with our samples. In this study, a few large-sized aggregates were also observed as demonstrated by the high intensity-low number DLS peaks at higher hydrodynamic diameters (Fig. S4, ESI†).

Results for the effective particle diameter (using the Stokes–Einstein equation) corroborate the adsorption of Fetuin-A onto the aggregated $CaCO_3$ structures. Fig. 7A shows an increase in the effective diameter of the $CaCO_3$ nanoparticle aggregates from the adsorption of the much smaller Fetuin-A. Moreover, changes in zeta potential are indicators of protein adsorption, as discussed elsewhere.[61] For $CaCO_3$ nanoparticles, a very stable zeta potential of −24.2 ± 1.8 mV was observed. However, after Fetuin-A/$CaCO_3$ complexes formation, an increase in surface charge was obtained (−0.1 ± 9 mV), confirming the Fetuin-A adsorption process on $CaCO_3$ in DMEM.

Interestingly, after an incubation time of four days at ambient temperature and no further mechanical treatment, a decrease in the effective diameter was observed. This size decrease at longer incubation times supports the stabilization of the Fetuin-A/$CaCO_3$ complexes[62] followed by removal of calcium from the interior, as was indicated by TEM (Fig. 6C). Thus, Fetuin-A not only inhibits further growth of the $CaCO_3$ nanoparticle aggregate, it also potentially aids in the solubilisation and dispersal of the calcite form of $CaCO_3$ over time (Fig. 7B and Fig. S4, ESI†). To further confirm this result, a control experiment without Fetuin-A was performed in which DMEM and $CaCO_3$ particles were incubated for 4 days (Fig. 7B).

Results showed an increase in effective diameter for the $CaCO_3$ particles when Fetuin-A is not present; therefore, the decrease in $CaCO_3$ diameter is attributed to the presence of Fetuin-A. Additional control experiments are discussed in ESI2 (Fig. S4 and S5, ESI†). UV-Vis spectroscopy has been previously utilized to study the adsorption mechanisms of proteins on different substrates,[63] and was used in this study to compare neat $CaCO_3$ particles to Fetuin-A/$CaCO_3$ complexes in solution. The UV-Vis results confirm adsorption of Fetuin-A onto the $CaCO_3$ particles, as shown by a slight shift in maximum molecular absorbance as compared to neat Fetuin-A (Fig. S6, ESI†); these results are discussed in more detail in ESI3.†

3. Conclusions

In this study, Fetuin-A has been shown to adsorb, stabilize and bind, and chemically and morphologically modify calcium carbonate particles in a simulated body fluid (DMEM). These results are important since calcium carbonate plays a significant role in current drug delivery applications and biomineralization, and is becoming an attractive material for future pharmaceutical and biomedical applications. Results obtained in this study can be used to evaluate of the role and impact of Fetuin-A when in the presence of $CaCO_3$ calcite particles, and extends prior studies on how Fetuin-A affects hydroxyapatite formation. The chemical and physical characterizations of calcite calcium carbonate ($CaCO_3$), the glycoprotein Fetuin-A, and Fetuin-A/$CaCO_3$ complexes provide the basis for further studies examining the functional group involved in short- and long-term interactions. It has been shown that Fetuin-A can stabilize the calcium ions present in $CaCO_3$ particles without the presence of a phosphate ion, as has been purported elsewhere. The Fetuin-A/$CaCO_3$ complexes have been shown to be time-sensitive, with the mechanism including an initial adsorption, followed by a complex stabilization period, and then destabilization and removal of the calciprotein particles. This mechanism has been explored using SEM and TEM to examine the morphological/structural changes, FTIR and XPS for chemical characterization, and DLS, cryo TEM and UV-Vis for *in situ* characterization of the complex formation and evolution. The characterization methods presented in this study can be applied to the study of other protein-substrate interactions, including more commonly studied minerals such as calcium phosphate salts. The results from this study show that Fetuin-A has potential as a native glycoprotein which can be useful in the development of biomedical therapeutics by stabilizing inorganic particles that are currently being explored as drug delivery vehicles.

4. Experimental section

4.1 Materials

Human Fetuin-A was used as-received and reconstituted to a concentration of 0.1 mg mL^{-1} (Sigma-Aldrich, St. Louis, MO; Biovendor, Asheville, NC). After preparation, Dulbecco's modified Eagle's medium (DMEM) (Corning, Lowell, MA) was filtered prior to use with a cellulose nitrate 0.22 μm pore membrane (Corning) followed by a 0.1 μm Acrodisc® Supor® membrane. By using double filtered, large particles were separated from the fluid media, allowing to characterize only the $CaCO_3$ nanoparticles. DI water was used from an EMD millipore water purification system (type I reagent grade water). Calcium carbonate ($CaCO_3$) nanoparticles (15–40 nm) were used as-received and without any further modification (SkySpring Nanomaterials, Inc., TX, USA).

4.2 Fetuin-A/$CaCO_3$ nanoparticle complex formation

For the Fetuin-A/$CaCO_3$ particles used in this work, DMEM was the solvent for all solutions. After two-stage DMEM filtering procedures, as discussed in the Section 4.1, a small aliquot of DMEM was examined with DLS to guarantee a zero effective diameter and a clean DMEM fluid media for $CaCO_3$ *in situ* studies. Then, a solution with a concentration of 0.1 mg mL^{-1} of $CaCO_3$ in DMEM was prepared (4 mL). This solution was then filtered using an Acrodisc® 1.2 μm Versapor® membrane syringe filter, and sonicated for 5 minutes using a sonication bath (VWR) without heating. After sonication, DLS measurements were performed and the effective diameter of the sample was recorded. Fetuin-A protein (100 μL) was then added, approximately after 15 min after initial $CaCO_3$ solution preparation, at a concentration of 100 μg mL^{-1}. This solution containing $CaCO_3$ and Fetuin-A in DMEM was then studied using DLS, TEM, FTIR, XPS, UV-Vis, and SEM to examine the formation and evolution of the Fetuin-A/$CaCO_3$ complexes.

4.3 Chemical characterization

A Nicolet 6700 FTIR spectrophotometer (Thermo Electron Corporation) with a He–Ne laser, MCT-A* detector, and KBr beamsplitter with a Miracle-ATR™ accessory (Diamond-ZnSe crystal, PIKE Technologies) was used for ATR-FTIR spectra collection. Fetuin-A, $CaCO_3$, and Fetuin-A/$CaCO_3$ nanoparticle complexes samples were deposited onto the ATR crystal from solution, the solvent was allowed to dry, leaving a thin sample film on the crystal's surface. Infrared spectral data was then collected and analyzed using Omnic software (v8.1.10, 1992-2009, Thermo Fisher Scientific, Inc.), and a minimum of 256 scans collected for each sample. X-ray photoelectron spectroscopy (XPS) was conducted using a PHI 1600 XPS surface analysis system (Physical Electronics, Mg K_α X-ray source (300 W, 15 kV), 45°

take-off angle, PHI 10-360 spherical capacitor energy analyzer, and an Omni Focus II small-area lens). All samples were deposited from solution onto a clean gold-coated silicon wafer substrate. A total of 10 scans with 26.95 eV pass energy across the 1100–0 eV range were analyzed for survey scans. High-resolution XPS spectra consist of a minimum of 25 scans, at a 23.5 eV pass energy and 0.1 eV step size. At least three spectra per sample were analyzed, and the averages are reported. Data analysis was performed using Origin Pro 2015.

4.4 Morphological characterization

Scanning electron microscopy (SEM) was performed using a JEOL JSM-6500 field emission scanning electron microscope (FE-SEM) operated at 5 or 15 keV. Sample preparation was performed in a similar manner to the XPS analysis; however, the gold-coated silicon wafers were mounted on SEM holders using double-sided black carbon tape. High-resolution transmission electron microscopy (TEM) images were obtained using a JEOL 2100 at 200 kV. For TEM, sample droplets were placed on a carbon Formvar Cu grid 300 mesh (Electron Microscopy Science), and the liquid was evaporated at ambient conditions inside a fume hood. Cryo TEM images were collected using a JEOL 1400 Biological TEM with a Gatan Cryoplunge™ adapter.

4.5 Particle diameters

Dynamic light scattering (DLS) and zeta-potential phase-angle light scattering (PALS) measurements were conducted using a ZetaPALS instrument (659 nm wavelength, 90° detector, Brookhaven Instruments Corporation (BIC), Holtsville, NY). At least 5 measurements were taken for each sample, including 30 measurement cycles for each PALS experiment. Outlier analysis was performed at a 0.05 level of significance using Grubb's test. Samples were analyzed at ambient temperature conditions (~22 °C). Results reported are based on Stokes–Einstein equation for the effective hydrodynamic diameter, or average mean diameter by number, and is specified for each analysis.

4.6 Protein adsorption studies

A Shimadzu 2550 UV-Vis spectrometer was utilized for the analysis of the Fetuin-A glycoprotein and its adsorption onto aggregated calcium carbonate nanoparticles. Filtered DMEM was used as the blank.

Acknowledgements

This work was funded by the National Science Foundation (EPS-0903787; IIA-1430364) and the Mississippi INBRE (IDEA Network for Biomedical Research Excellence). DLS and TEM instrumentation was provided by NSF grants EPS-0903787 and DBI-1126743, respectively. We are very grateful to Ying Xiao and Dr Clayton Loehn at Louisiana State University for assisting in some of the TEM work presented in this study, and to Dr I-Wei Chu at Institute for Imaging and Technical Technologies (I2AT) at Mississippi State University for her assistance with some of the SEM and TEM imaging.

References

1 S. K. L. Levengood and M. Zhang, *J. Mater. Chem. B*, 2014, **2**, 3161–3184.
2 L. K. Grunenfelder, N. Suksangpanya, C. Salinas, G. Milliron, N. Yaraghi, S. Herrera, K. Evans-Lutterodt, S. R. Nutt, P. Zavattieri and D. Kisailus, *Acta Biomater.*, 2014, **10**, 3997–4008.
3 E. S. Vasquez, I. W. Chu and K. B. Walters, *Langmuir*, 2014, **30**, 6858–6866.
4 J. Sun, C. Chen, H. Pan, Y. Chen, C. Mao, W. Wang, R. Tang and X. Gu, *J. Mater. Chem. B*, 2014, **2**, 4544–4553.
5 A. Schulz, H. Wang, P. van Rijn and A. Boker, *J. Mater. Chem.*, 2011, **21**, 18903–18918.
6 M. W. Trim, M. F. Horstemeyer, H. Rhee, H. El Kadiri, L. N. Williams, J. Liao, K. B. Walters, J. McKittrick and S.-J. Park, *Acta Biomater.*, 2011, **7**, 1228–1240.
7 L. K. Grunenfelder, S. Herrera and D. Kisailus, *Small*, 2014, **10**, 3207–3232.
8 C. Tan, Z. Sun, Y. Hong, Y. Li, X. Chen and X. Zhang, *J. Mater. Chem. B*, 2013, **1**, 3694–3704.
9 D. Wei, W. Xiao, J. Sun, M. Zhong, L. Guo, H. Fan and X. Zhang, *J. Mater. Chem. B*, 2015, **3**, 2753–2763.
10 E. Abdullayev and Y. Lvov, *J. Mater. Chem. B*, 2013, **1**, 2894–2903.
11 Q. Ruan and J. Moradian-Oldak, *J. Mater. Chem. B*, 2015, **3**, 3112–3129.
12 L. L. Demer and Y. Tintut, *Circulation*, 2008, **117**, 2938–2948.
13 X. Wang, C. Wu, K. Tao, K. Zhao, J. Wang, H. Xu, D. Xia, H. Shan and J. R. Lu, *J. Phys. Chem. B*, 2010, **114**, 5301–5308.
14 R. K. DeLong, C. M. Reynolds, Y. Malcolm, A. Schaeffer, T. Severs and A. Wanekaya, *Nanotechnol., Sci. Appl.*, 2010, **3**, 53–63.
15 W. Zhu, J. Lin, C. Cai and Y. Lu, *J. Mater. Chem. B*, 2013, **1**, 841–849.
16 J. Lee and H.-S. Yun, *J. Mater. Chem. B*, 2014, **2**, 1255–1263.
17 Y. Yamamoto, T. Nishimura, A. Sugawara, H. Inoue, H. Nagasawa and T. Kato, *Cryst. Growth Des.*, 2008, **8**, 4062–4065.
18 A. Heiss, A. DuChesne, B. Denecke, J. Grötzinger, K. Yamamoto, T. Renneé and W. Jahnen-Dechent, *J. Biol. Chem.*, 2003, **278**, 13333–13341.
19 W. Jahnen-Dechent, C. Schäfer, M. Ketteler and M. McKee, *J. Mol. Med.*, 2008, **86**, 379–389.
20 V. Persy and P. D'Haese, *Trends Mol. Med.*, 2009, **15**, 405–416.
21 A. Pasch, S. Farese, S. Graber, J. Wald, W. Richtering, J. Floege and W. Jahnen-Dechent, *J. Am. Soc. Nephrol.*, 2012, **23**, 1744–1752.
22 J. Wald, S. Wiese, T. Eckert, W. Jahnen-Dechent, W. Richtering and A. Heiss, *Soft Matter*, 2011, **7**, 2869–2874.
23 M.-Q. Gong, J.-L. Wu, B. Chen, R.-X. Zhuo and S.-X. Cheng, *Langmuir*, 2015, **31**, 5115–5122.

24 C. Qi, Y.-J. Zhu and F. Chen, *ACS Appl. Mater. Interfaces*, 2014, **6**, 4310–4320.
25 W. Wei, G.-H. Ma, G. Hu, D. Yu, T. McLeish, Z.-G. Su and Z.-Y. Shen, *J. Am. Chem. Soc.*, 2008, **130**, 15808–15810.
26 L. Brylka and W. Jahnen-Dechent, *Calcif. Tissue Int.*, 2013, **93**, 355–364.
27 M. Mihai, F. Bucătariu, M. Aflori and S. Schwarz, *J. Cryst. Growth*, 2012, **351**, 23–31.
28 A. Haglund, B. Ek and P. Ek, *Biochem. J.*, 2001, **357**, 437–445.
29 J. T. Lee, Y. Leng, K. L. Chow, F. Ren, X. Ge, K. Wang and X. Lu, *Acta Biomater.*, 2011, **7**, 2615–2622.
30 T. Kokubo and H. Takadama, *Biomaterials*, 2006, **27**, 2907–2915.
31 A. C. Tas, *Acta Biomater.*, 2014, **10**, 1771–1792.
32 E. Foran, S. Weiner and M. Fine, *Sci. Rep.*, 2013, **3**, 1700.
33 J. D. Rodriguez-Blanco, S. Shaw and L. G. Benning, *Nanoscale*, 2011, **3**, 265–271.
34 M. A. Legodi, D. de Waal, J. H. Potgieter and S. S. Potgieter, *Miner. Eng.*, 2001, **14**, 1107–1111.
35 Z. Ganim, H. S. Chung, A. W. Smith, L. P. DeFlores, K. C. Jones and A. Tokmakoff, *Acc. Chem. Res.*, 2008, **41**, 432–441.
36 A. Barth, *Biochim. Biophys. Acta, Bioenerg.*, 2007, **1767**, 1073–1101.
37 G. Steiner, S. Tunc, M. Maitz and R. Salzer, *Anal. Chem.*, 2007, **79**, 1311–1316.
38 R. Podila, R. Chen, P. C. Ke, J. M. Brown and A. M. Rao, *Appl. Phys. Lett.*, 2012, **101**, 263701.
39 M. M. Patel, J. D. Smart, T. G. Nevell, R. J. Ewen, P. J. Eaton and J. Tsibouklis, *Biomacromolecules*, 2003, **4**, 1184–1190.
40 C. Gruian, E. Vanea, S. Simon and V. Simon, *Biochim. Biophys. Acta, Proteins Proteomics*, 2012, **1824**, 873–881.
41 T. L. Barr and S. Seal, *J. Vac. Sci. Technol., A*, 1995, **13**, 1239–1246.
42 S. L. Stipp and M. F. Hochella Jr, *Geochim. Cosmochim. Acta*, 1991, **55**, 1723–1736.
43 W. J. Landis and J. R. Martin, *J. Vac. Sci. Technol., A*, 1984, **2**, 1108–1111.
44 T. L. Barr and S. Seal, *J. Vac. Sci. Technol., A*, 1995, **13**, 1239–1246.
45 B. G. Russell, W. E. Moddeman, J. C. Birkbeck, S. E. Wright, D. S. Millington, R. D. Stevens and K. E. Dombrowski, *Biospectroscopy*, 1998, **4**, 257–266.
46 S. Ray and A. G. Shard, *Anal. Chem.*, 2011, **83**, 8659–8666.
47 E. Vanea, K. Magyari and V. Simon, *J. Optoelectron. Adv. Mater.*, 2010, **12**, 1206.
48 L. D. Setiawan, H. Baumann and D. Gribbin, *Surf. Interface Anal.*, 1985, **7**, 188–195.
49 I. Carvalho, R. E. Galindo, M. Henriques, C. Palacio and S. Carvalho, *J. Phys. D: Appl. Phys.*, 2014, **47**, 335401.
50 N. A. J. M. Sommerdijk and G. d. With, *Chem. Rev.*, 2008, **108**, 4499–4550.
51 A. Heiss, W. Jahnen-Dechent, H. Endo and D. Schwahn, *Biointerphases*, 2007, **2**, 16–20.
52 A. Heiss, T. Eckert, A. Aretz, W. Richtering, W. Van Dorp, C. Schäfer and W. Jahnen-Dechent, *J. Biol. Chem.*, 2008, **283**, 14815–14825.
53 P. A. Price, G. R. Thomas, A. W. Pardini, W. F. Figueira, J. M. Caputo and M. K. Williamson, *J. Biol. Chem.*, 2002, **277**, 3926–3934.
54 K. Mori, M. Emoto and M. Inaba, *Recent Pat. Endocr., Metab. Immune Drug Discovery*, 2011, **5**, 124–146.
55 W. Jahnen-Dechent, A. Heiss, C. Schafer and M. Ketteler, *Circ. Res.*, 2011, **108**, 1494–1509.
56 L. B. Gower, *Chem. Rev.*, 2008, **108**, 4551–4627.
57 F. Nudelman, K. Pieterse, A. George, P. H. H. Bomans, H. Friedrich, L. J. Brylka, P. A. J. Hilbers, G. de With and N. A. J. M. Sommerdijk, *Nat. Mater.*, 2010, **9**, 1004–1009.
58 L. Addadi and S. Weiner, *Proc. Natl. Acad. Sci. U. S. A.*, 1985, **82**, 4110–4114.
59 L. Gago-Duport, M. J. I. Briones, J. B. Rodríguez and B. Covelo, *J. Struct. Biol.*, 2008, **162**, 422–435.
60 Q. Zhang, S.-J. Liu and S.-H. Yu, *J. Mater. Chem.*, 2009, **19**, 191–207.
61 K. Rezwan, A. R. Studart, J. Vörös and L. J. Gauckler, *J. Phys. Chem. B*, 2005, **109**, 14469–14474.
62 P. A. Price and J. E. Lim, *J. Biol. Chem.*, 2003, **278**, 22144–22152.
63 K. Siriwardana, M. Gadogbe, S. M. Ansar, E. S. Vasquez, W. E. Collier, S. Zou, K. B. Walters and D. Zhang, *J. Phys. Chem. C*, 2014, **118**, 11111–11119.